Computational Framework for Durability Design and Assessment of Reinforced Concrete Structures Exposed to Chloride Environment

Gang Lin[1], Yinghua Liu[1,2] and Zhihai Xiang[1]

Abstract: Deterioration of reinforced concrete (RC) structures due to chloride ingress followed by reinforcement corrosion is a serious problem all over the world, therefore prediction of chloride profiles is a key element in evaluating durability and integrity of RC structures exposed to chloride environment. In the present paper, an integrated finite element-based computational framework is developed for predicting service life of RC structures exposed to chloride environment, which takes environment temperature and humidity fluctuations, diffusion and convection, chloride binding, as well as the decay of durability of structures caused by coupled deterioration processes into account. The decay of RC structures due to environment loadings and service loadings is considered in a coupled thermo-hygro-mechanical model. Based on the conservation of energy and mass, the governing equations of heat transfer, moisture transport and chloride ingress into partially saturated concrete are described particularly. Employing the Galerkin finite element method for the spatial discretization and a finite difference time-stepping scheme for the temporal discretization, a fully implicit algorithm is developed for the numerical solutions of the governing equations. The computational framework is implemented and validated by comparing numerical results with analytical solutions and experimental observations. Further numerical simulations have been carried out for quantitative durability design and assessment of RC structures exposed to chloride environment.

Keywords: computational framework, durability design and assessment, chloride environment, partially saturated concrete, diffusion and convection, coupled deterioration processes

---

[1] Department of Engineering Mechanics, AML, Tsinghua University, Beijing 100084, China

[2] Corresponding author, Tel: +86-10-62773751; fax: +86-10-62781824; Email: yh-liu@mail.tsinghua.edu.cn

1 Introduction

Degradation of RC structures due to physical and chemical attack is a major topic in civil engineering [Ciampoli (1999); Bangert, Grasberger, Kuhl, and Meschke (2003); Petryna and Kratzig (2005)]. One of the main causes of deterioration of RC structures is ascribed to chloride-induced corrosion of reinforcement which is becoming a serious problem all over the world, therefore service life prediction of RC structures exposed to chloride environment is of great importance in practice. A large amount of work done on service life modeling associated with chloride-induced corrosion has taken diffusion as the main transport mechanism of chloride ions into concrete under the assumption that the concrete cover is fully saturated [Masi, Colella, Radaelli and Bertolini (1997); Samson, Marchand, Robert and Bournazel (1999)]. In reality, concrete is often found in a partially saturated condition rather than a fully saturated condition, such as the case of RC structures exposed to de-icing salts or the case of the splash and tide zones of RC structures exposed to marine environment. When a nonsaturated concrete surface is being wet, the moisture is quickly absorbed into concrete through capillary suction bringing with itself dissolved chloride ions. During dry periods, the moisture at the concrete surface evaporates leaving the chloride ions behind in the concrete pore solution. Due to these two phenomena, the chloride concentration reaches a maximum value some millimeters inside the concrete. In order to model mass transport under combined diffusion and convection mechanisms, some researchers employed the continuous Galerkin finite element method [Ferguson and Palananthakumar (2005); Selvadurai and Dong (2006); Kringos, Scarpas, and Selvadurai (2008)] or meshless local Petrov-Galerkin (MLPG) method [Lin and Atluri (2000); Golberg and Chen (2001); Mohammadi (2008)], or the boundary-integral-equation method (BIEM) [Mai-Duy, Tran-Cong and Tanner (2006)], or the boundary element method [Simoes and Tadeu (2005); Romero and Benitez (2008)], or the discontinuous Galerkin (DG) finite element method [Gomez, Colominas, Navarrina and Casteleiro (2007)] to solve the diffusion-convection problem. Some numerical models were developed to model chloride penetration into non-saturated structures [Saetta, Scotta and Vitaliani (1993); Ababneh, Benboudjema and Xi (2003)]. Despite these efforts, some discrepancies between the predicted values and the observed data from laboratory and field still exist. This may be attributed to particularity of this problem such as the difference of moisture transport into concrete during drying-wetting cycles, the fluctuation of external environment and the interactions between mass transport and decay of RC structures, etc.

The durability of RC structures will decay gradually when exposed to various physical, chemical and mechanical deterioration processes [Gawin, Pesavento and Schrefler (2006a, 2006b); Roels, Moonen, Proft and Carmeliet (2006); Chen and

Mahadevan (2007)]. The porosity and permeability of concrete are increased due to the coupled deterioration processes, and the transport rates of various aggressive agents into concrete are accelerating accordingly [Tabrez, Mitra and Gopalakrishnan (2007); Chen, Gan and Chen (2008)]. In turn, the durability of RC structures decays further due to the accelerating deterioration processes. The coupling between mass transport and these deterioration processes is becoming increasingly necessary to be considered in durability design and assessment. Most previous research, however, was focused on modeling service life of undamaged concrete. Subsequently, some work was conducted to address the influence of cracking and sustained loading on the penetration resistance or permeability of concrete [Francois and Maso (1988); Samaha and Hover (1992); Aldea, Shah and Karr (1999); Djerbi, Bonnet, Khelidj and Baroghel-bouny (2008)]. Comparatively little work has been performed to quantitatively describe how these properties change when exposed to coupled deterioration processes and how the decay of concrete structures accelerates mass penetration into concrete structures accordingly, which frequently occur in field applications.

The main purpose of the present paper is to develop a computational framework for predicting service life of RC structures exposed to chloride environment, which takes environment temperature and humidity fluctuations, difference of moisture transport into concrete during drying-wetting cycles, chloride binding, as well as the decay of durability of structures into account. In the present computational framework, both the diffusion and convection mechanisms are considered to model chloride into partially saturated concrete. The interactions between mass transport and the decay of RC structures under coupled deterioration processes are taken into account in a coupled thermal-hygro-mechanical model, and a scalar damage index will be adopted here to characterize the alteration of porosity and permeability of concrete under multiple coupled deterioration processes. The heat transfer, moisture transport and chloride penetration processes are formulated using the governing partial differential equations on the basis of energy and mass conservation. Using the Galerkin finite element method and applying a finite difference time-steeping scheme, a fully implicit algorithm has been developed for the numerical solution of the partial differential equations. The validation and accuracy of the implemented computational framework are demonstrated by comparing numerical solutions with analytical results and experiment observations. Finally, the application of the present computational framework is demonstrated by predicting service life of RC structures exposed to chloride environment.

2   Basic formulation

Based on the conservation of energy and mass, the governing equations of heat transfer, moisture transport and chloride penetration into partially saturated concrete have the same general form [Martín-Pérez, Pantazopoulou and Thomas (2001)]:

$$\lambda \frac{\partial \varphi}{\partial t} + \underbrace{\mathrm{div}\,(\mathbf{J})}_{\text{diffusion}} + \underbrace{\mathrm{div}\,(\mathbf{J}')}_{\text{convection}} = 0 \tag{1}$$

The correspondence between Eq. (1) and different governing field equations is shown in Table 1. The physical aspects of these equations are described in detail in the following.

Table 1: Correspondence between Eq. (1) and transport differential equations

Physical problem	φ	λ	$\mathbf{J}$	$\mathbf{J}'$
Heat transfer	T	ρc	$-\kappa \mathrm{grad}\,(T)$	0
Moisture transport	θ	1	$-D_\theta \mathrm{grad}\,(\theta)$	0
Chloride ingress	C_{fc}	$\frac{\partial C_{\mathrm{tc}}}{\partial C_{\mathrm{fc}}}$	$-sD_c \mathrm{grad}\,(C_{\mathrm{fc}})$	$-sC_{\mathrm{fc}}D_\theta \mathrm{grad}\,(\theta)$

In the heat transfer analysis, the thermal conductivity κ, the mass density ρ and the specific heat capacity c vary tinily and can be assumed to be constants which have been confirmed by other researchers [Martín-Pérez, Pantazopoulou and Thomas (2001); Isgor and Razaqpur (2004)]. In this case, the governing differential equation of heat transfer may be solved firstly without considering the influences of other mass transport processes.

In the moisture diffusion analysis, θ is the water saturation degree in the concrete pores, and D_θ is the moisture diffusivity. When a partially saturated concrete surface is being wet, the moisture is quickly absorbed through capillary suction. During dry periods, the moisture is driven out from the inside concrete by pore water evaporation. Thus the moisture diffusivity D_θ in Table 1 during drying and wetting periods should differ [Janssen, Blocken and Carmeliet (2007)]:

$$D_\theta = \begin{cases} D_d\,(\theta) = D_d^s \left[\alpha_0 + \left(\alpha_0 + \frac{1-\alpha_0}{1+\left(\frac{1-\theta}{1-\theta_c}\right)^N} \right) \right] & \text{during drying period} \\ D_w\,(\theta) = D_w^0 \exp\,(n\theta_r) & \text{during wetting period} \end{cases} \tag{2}$$

where D_d^s is the drying moisture diffusivity when totally saturated, and α_0, θ_c and N are model parameters ($\alpha_0 = 0.05$, $\theta_c = 0.792$, $N = 6$[Wong, Wee, Swaddiwudhipong and Lee (2001)]); D_w^0 is the wetting moisture diffusivity at an initial water

saturation degree of θ_0, n is an empirically determined constant ($n = 6$[Wong, Wee, Swaddiwudhipong and Lee (2001)]), and $\theta_r = \theta - \theta_0/\theta_1 - \theta_0$ is the normalized water saturation degree where θ_1 is the water saturation degree of totally saturated concrete. To reflect the dependence of moisture diffusivity D_θ on the level of temperature T, degree of hydration of concrete characterized by an equivalent hydration period t_e and the decay of concrete structures' durability characterized by a scalar damage variable d, the multifactor law is adopted herein [Bazant and Najjar (1972); Gerard, Pijaudier-Cabot and Laborderie (1998)]:

$$
D_\theta = \begin{cases} D_d\left(\theta\right) = D_d^s\left(\alpha_0 + \dfrac{1-\alpha_0}{1+\left(\frac{1-\theta}{1-\theta_c}\right)^N}\right) F_1\left(T\right) F_2\left(t_e\right) F_3\left(d\right) & \text{during drying period} \\[2em] D_w\left(\theta\right) = D_w^0 \exp\left(n\theta_r\right) F_1\left(T\right) F_2\left(t_e\right) F_3\left(d\right) & \text{during wetting period} \end{cases}
$$

(3)

where $F_1\left(T\right)$, $F_2\left(t_e\right)$ and $F_3\left(d\right)$ respectively account for the dependence of D_θ on the temperature level T, the degree of hydration characterized by an equivalent hydration period t_e and the decay of concrete structures' durability characterized by a scalar damage variable d, and can be described as follows:

$$
F_1\left(T\right) = \exp\left[\frac{U_\theta}{R} \cdot \left(\frac{1}{T_{\text{ref}}} - \frac{1}{T}\right)\right]
$$

(4a)

$$
F_2\left(t_e\right) = 0.3 + \sqrt{\frac{13}{t_e}}
$$

(4b)

$$
F_3\left(d\right) = 1 + \frac{D_{\theta,\,\text{max}}}{D_{\theta,\,\text{ref}}}\left[1 - \frac{1}{1 + \left(\frac{d}{d_{\text{cr}}}\right)^{nn}}\right]
$$

(4c)

where U_θ is the activation energy of the moisture diffusion process, R is the gas constant, T_{ref} is the reference temperature at which the reference moisture diffusivity is determined, nn and d_{cr} are model parameters ($nn = 5$, $d_{\text{cr}} = 0.4$ [Gerard, Pijaudier-Cabot and Laborderie (1998)]), and the value of $D_{\theta,max}/D_{\theta,ref}$ is chosen to be 20 [Cerny, Drchalova and Rovnanikova (2001)].

Chloride penetration into partially saturated concrete is a complex phenomenon, involving various factors such as diffusion of chloride ions and movement of chloride ions due to permeation of water in concrete. As Table 1 shows, the diffusive chloride ion flux $\mathbf{J}$ can be expressed as follows:

$$
\mathbf{J} = -sD_c \text{grad}\left(C_{\text{fc}}\right)
$$

(5)

and the convective chloride ion flux $\mathbf{J}'$ can be mathematically expressed as:

$$
\mathbf{J}' = -sC_{\text{fc}}D_\theta \text{grad}\left(\theta\right)
$$

(6)

Chloride ions in concrete can be either dissolved in the pore solution (free chloride), or chemically and physically bound to the cement hydrates and their surfaces (bound chloride), and only the free chloride ions dissolved in the pore solution are responsible for initiating the process of corrosion [Martín-Pérez, Zibara, Hooton and Thomas (2000)]. The binding properties of a specific cementitious system are usually defined in the form of a binding isotherm, with the amount of bound chloride C_{bc} expressed as a function of the free chloride concentration C_{fc}. The total, bound and free chloride concentrations in concrete are related by:

$$C_{tc} = C_{bc} + s\theta C_{fc} \tag{7}$$

where C_{tc} is the total chloride concentration in concrete, s is the porosity of concrete. In the present paper, Freundlich binding isotherm will be chosen to describe the relationship between bound chloride and free chloride, and can be written as follows [Tang and Nilsson (1993)]:

$$C_{bc} = \alpha C_{fc}^{\beta} \tag{8}$$

where α and β are model parameters.

To reflect the dependence of chloride diffusion coefficient D_c on temperature, time of exposure, water saturation degree and the decay of concrete structures' durability, the effective chloride diffusion coefficient $D_{c,\,ref}$ of concrete, determined under some defined reference conditions, can be modified as follows [Saetta, Scotta and Vitaliani (1993); Gerard, Pijaudier-Cabot and Laborderie (1998)]:

$$D_c = D_{c,\,ref} \cdot f_1(T) \cdot f_2(t) \cdot f_3(\theta) \cdot f_4(d) \tag{9}$$

where $f_1(T)$, $f_2(t)$, $f_3(\theta)$ and $f_4(d)$ respectively account for the dependence of D_c on temperature T, time of exposure t, water saturation degree θ, and the decay of concrete structures' durability characterized by d, and can be described as follows [Saetta, Scotta and Vitaliani (1993); Gerard, Pijaudier-Cabot and Laborderie (1998)]:

$$f_1(T) = \exp\left[\frac{U_c}{R}\left(\frac{1}{T_{ref}} - \frac{1}{T}\right)\right] \tag{10a}$$

$$f_2(t) = \left(\frac{t_{ref}}{t}\right)^m \tag{10b}$$

$$f_3(\theta) = \theta^{\eta} \tag{10c}$$

$$f_4(d) = 1 + \frac{D_{c,max}}{D_{c,ref}}\left[1 - \frac{1}{1 + \left(\frac{d}{d_{cr}}\right)^{nn}}\right] \tag{10d}$$

where U_C is the activation energy of the chloride diffusion process, t_{ref} is the time of concrete exposure at which $D_{c, ref}$ is measured, m is the age reduction factor ($m = 0.6$ [Saetta, Scotta and Vitaliani (1993)]) , η is the power index, nn and d_{cr} are model parameters ($nn = 5$, $d_{cr} = 0.4$ [Gerard, Pijaudier-Cabot and Laborderie (1998)]), and the value of $D_{c,max}/D_{c,ref}$ is chosen to be 8 [Gerard and Marchand (2000)].

3 Decay of RC structures' durability

Most deterioration processes are able to alter the porosity and permeability of concrete, and result in accelerating aggressive agents' penetration into RC structures. In turn, the durability of RC structures decays further due to the accelerating deterioration processes. The interactions between these deterioration processes and mass transport are becoming increasingly necessary to be considered in durability design and assessment. Three typical deterioration processes, i.e. heat conduction and associated thermal contraction/expansion, moisture transfer and associated drying shrinkage/wetting expansion, and mechanical deterioration due to service loadings, which frequently occur in field applications, are taken into account herein to study the influences of the decay of RC structures' durability on service life of RC structures.

In the present paper, the interactions between mass transport and the deterioration processes are taken into account in a coupled thermo-hygro-mechanical model. In this model, the coupled system of mechanical deformation, moisture transport and heat conduction is characterized by the displacement field $\mathbf{u}$, the water saturation degree θ, and the temperature T together with a set of internal variables. The primary variables in the domain Ω are controlled by the balance of linear momentum, mass content and energy as:

$$\text{div}(\sigma) = 0$$
$$\frac{\partial \theta}{\partial t} = \text{div}[D_\theta \text{grad}(\theta)] \tag{11}$$
$$\rho c \frac{\partial T}{\partial t} = \text{div}[\kappa \text{grad}(T)]$$

In general, the total strain $\boldsymbol{\varepsilon}_{tot}$ of concrete structures under environment loadings (i.e. moisture and heat) and service loadings can be split into the following components:

$$\boldsymbol{\varepsilon}_{tot} = \boldsymbol{\varepsilon}_{me} + \boldsymbol{\varepsilon}_{th} + \boldsymbol{\varepsilon}_{sh} \tag{12}$$

where $\boldsymbol{\varepsilon}_{me}$ means mechanical strain caused by both service loadings and environment loadings, $\boldsymbol{\varepsilon}_{th} = \alpha_T \Delta T \mathbf{I}$ is thermal strain, α_T is the thermal expansion coeffi-

cient of concrete and $\mathbf{I}$ is unit tensor of second-order; $\boldsymbol{\varepsilon}_{\mathrm{sh}} = \beta_{\mathrm{sh}}\Delta W \mathbf{I}$ is shrinkage strain, $W = s\theta$ is free moisture content of concrete and β_{sh} is the shrinkage coefficient of concrete.

In the thermo-hygro-mechanical model, the evolutions of plastic strain and damage variable usually be described in the effective stress space $\bar{\boldsymbol{\sigma}}$. The effective stress and plastic strain can be described as follows, respectively:

$$\bar{\boldsymbol{\sigma}} = \mathbf{D}_0^{\mathrm{el}} : \left(\boldsymbol{\varepsilon}_{\mathrm{tot}} - \boldsymbol{\varepsilon}_{\mathrm{th}} - \boldsymbol{\varepsilon}_{\mathrm{sh}} - \boldsymbol{\varepsilon}_{\mathrm{pl}}\right) \in \left\{\bar{\boldsymbol{\sigma}} | F\left(\bar{\boldsymbol{\sigma}}, \tilde{\boldsymbol{\varepsilon}}_{\mathrm{pl}}\right) \le 0\right\} \tag{13}$$

$$\dot{\boldsymbol{\varepsilon}}_{\mathrm{pl}} = \dot{\lambda} \frac{\partial F^p\left(\bar{\boldsymbol{\sigma}}\right)}{\partial \bar{\boldsymbol{\sigma}}} \tag{14}$$

where the initial elastic stiffness $\mathbf{D}_0^{\mathrm{el}}$ of concrete is a tensor of fourth-order, $\dot{\lambda}$ and F obey the Kuhn-Tucker conditions: $\dot{\lambda}F = 0, \dot{\lambda} \ge 0, F \le 0$. The yield function F is used herein to account for different evolution of strength under tension and compression in terms of effective stress [Lee and Fenves (1998); Cicekli, Voyiadjis and Abu Al-Rub (2007)]:

$$F\left(\bar{\boldsymbol{\sigma}}, \tilde{\boldsymbol{\varepsilon}}_{\mathrm{pl}}\right) = \frac{1}{1 - \alpha_p}\left(\sqrt{3\bar{J}_2} + \alpha_p\bar{I}_1 + \beta_p\left\langle\hat{\bar{\sigma}}_{\max}\right\rangle\right) - \bar{\sigma}_c\left(\tilde{\varepsilon}_{\mathrm{pl}}^c\right) \tag{15}$$

where $\bar{J}_2 = \bar{\mathbf{s}} : \bar{\mathbf{s}}/2$ is the second-invariant of the effective deviatoric stress, $\bar{\mathbf{s}} = \bar{\boldsymbol{\sigma}} - \bar{I}_1/3\mathbf{I}$, $\bar{I}_1 = \bar{\sigma}_{kk}$ is the first-invariant of the effective stress, $\hat{\bar{\sigma}}_{\max}$ is the maximum principal effective stress, and the Macauley bracket $\langle\cdot\rangle$ is defined by $\langle x\rangle = \frac{1}{2}\left(|x| + x\right)$. The parameters α_p and β_p are model constants which are defined as follows:

$$\alpha_p = \frac{f_{\mathrm{b0}} - f_{\mathrm{c0}}}{2f_{\mathrm{b0}} - f_{\mathrm{c0}}} \tag{16}$$

$$\beta_p = \frac{\bar{\sigma}_c\left(\tilde{\varepsilon}_{\mathrm{pl}}^c\right)}{\bar{\sigma}_t\left(\tilde{\varepsilon}_{\mathrm{pl}}^t\right)}\left(1 - \alpha_p\right) - \left(1 + \alpha_p\right) \tag{17}$$

where f_{b0} and f_{c0} are the initial biaxial and uniaxial compressive yield stresses, respectively. Typical experimental values of the ratio $f_{\mathrm{b0}}/f_{\mathrm{c0}}$ for concrete are in the range from 1.10 to 1.16, yielding values of α_p between 0.08 and 0.12. $\bar{\sigma}_t$ and $\bar{\sigma}_c$ are the effective tensile and compressive cohesion stresses, respectively. More detailed information about the yield function F can be found in the literature [Lee and Fenves (1998); Cicekli, Voyiadjis and Abu Al-Rub (2007)].

The plastic potential F^p is different from the yield function F (i.e. non-associated plastic flow) and therefore the direction of the plastic flow is not normal to F. The plastic potential F^p chosen for the present model is the Drucker-Prager function:

$$F^p = \sqrt{3\bar{J}_2} + \gamma_p\bar{I}_1 \tag{18}$$

where γ_p is the dilation constant.

The relationship between Cauchy stress and effective stress can be described as follows:

$$\boldsymbol{\sigma} = (1-d)\bar{\boldsymbol{\sigma}} \tag{19}$$

The scalar damage variable d is a function of stress state and two independent uniaxial damage variables d_t and d_c, and can be described as follows:

$$1 - d = (1 - s_t d_c)(1 - s_c d_t) \tag{20}$$

where s_t and s_c are functions of stress state, and d_t and d_c are respectively the uniaxial tension and compression damage variables which are assumed to be functions of equivalent plastic strains in tension and compression, respectively [Lee and Fenves (1998)]:

$$1 - d_t = \exp\left(-\kappa_t \tilde{\varepsilon}_{\mathrm{pl}}^t\right) \tag{21a}$$

$$1 - d_c = \exp\left(-\kappa_c \tilde{\varepsilon}_{\mathrm{pl}}^c\right) \tag{21b}$$

where κ_t and κ_c are material parameters identified from experimental stress-strain curves.

The evolution of the equivalent plastic strain is given by the expression of the form:

$$\tilde{\boldsymbol{\varepsilon}}_{\mathrm{pl}} = [\tilde{\varepsilon}_{\mathrm{pl}}^t, \tilde{\varepsilon}_{\mathrm{pl}}^c]^T \tag{22}$$

$$\dot{\tilde{\boldsymbol{\varepsilon}}}_{\mathrm{pl}} = \begin{bmatrix} \dot{\tilde{\varepsilon}}_{\mathrm{pl}}^t \\ \dot{\tilde{\varepsilon}}_{\mathrm{pl}}^c \end{bmatrix} = \begin{bmatrix} r(\hat{\bar{\boldsymbol{\sigma}}}) & 0 & 0 \\ 0 & 0 & -(1-r(\hat{\bar{\boldsymbol{\sigma}}})) \end{bmatrix} \begin{bmatrix} \hat{\dot{\varepsilon}}_{\mathrm{pl}}^1 \\ \hat{\dot{\varepsilon}}_{\mathrm{pl}}^2 \\ \hat{\dot{\varepsilon}}_{\mathrm{pl}}^3 \end{bmatrix} = \mathbf{h}(\hat{\bar{\boldsymbol{\sigma}}}, \tilde{\boldsymbol{\varepsilon}}_{\mathrm{pl}}) \cdot \begin{bmatrix} \hat{\dot{\varepsilon}}_{\mathrm{pl}}^1 \\ \hat{\dot{\varepsilon}}_{\mathrm{pl}}^2 \\ \hat{\dot{\varepsilon}}_{\mathrm{pl}}^3 \end{bmatrix} \tag{23}$$

where $r(\hat{\bar{\boldsymbol{\sigma}}}) = \dfrac{\sum\limits_{i=1}^{3} \langle \hat{\bar{\sigma}}_i \rangle}{\sum\limits_{i=1}^{3} |\hat{\bar{\sigma}}_i|}$ is a stress weight factor, $\hat{\bar{\sigma}}_i$ is the principal effective stress, and $\hat{\dot{\varepsilon}}_{\mathrm{pl}}^i$ is the eigenvalue of the plastic strain rate tensor and is ordered that $\hat{\dot{\varepsilon}}_{\mathrm{pl}}^1 \geq \hat{\dot{\varepsilon}}_{\mathrm{pl}}^2 \geq \hat{\dot{\varepsilon}}_{\mathrm{pl}}^3$.

4 Computational Framework

4.1 Scheme and implementation

The coupling between mass transport and various deterioration processes and the nonlinearity of material parameters involved make analytical solutions of Eq. (1)

impossible. In the present study, a finite element-based computational methodology is developed to simulate the coupling between mass transport and thermal-hygro-mechanical deterioration processes. To achieve this goal, the output of the computational framework at the *n*-th time step may be applied as input variable to modify the material properties at the $(n+1)$-th time step through the multifactor law. The flowchart of the simulation procedure is shown in Fig.1, which is illustrated as follows:
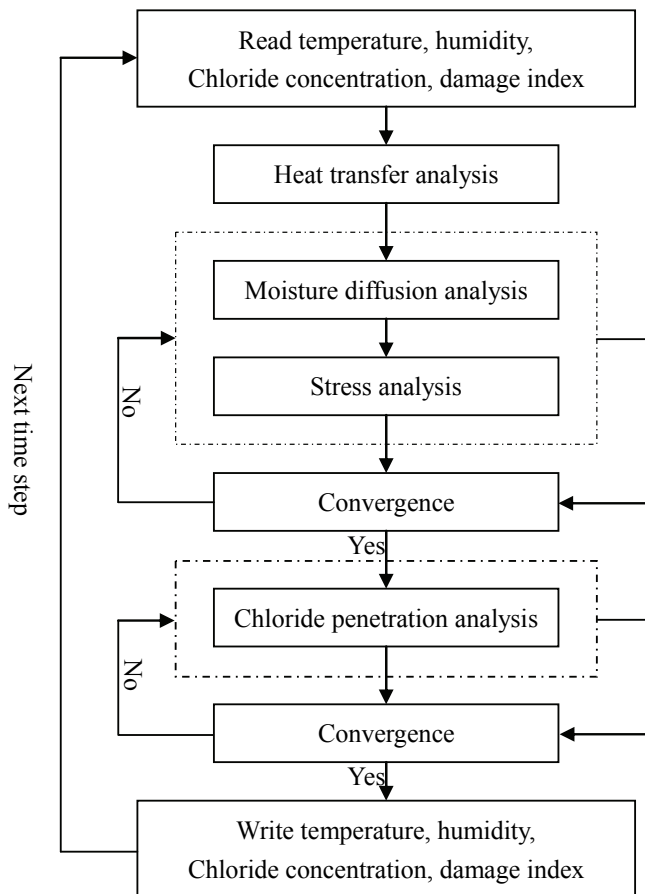
Figure 1: Flowchart of the computational framework

(i) Due to the insensitivity of thermal properties of concrete to moisture content and stress state [Martín-Pérez, Pantazopoulou and Thomas (2001); Isgor and Razaqpur (2004)], the transient heat transfer analysis is performed firstly and the spatial temperature distribution can be obtained accordingly, and the thermal strain $\boldsymbol{\varepsilon}_{n+1}^{\text{th}}$ at the

$(n+1)$-th time step can be undated accordingly:

$$\boldsymbol{\varepsilon}_{\text{th}}^{n+1} = \boldsymbol{\varepsilon}_{\text{th}}^{n} + \Delta\boldsymbol{\varepsilon}_{\text{th}} = \boldsymbol{\varepsilon}_{\text{th}}^{n} + \alpha_T dT\mathbf{I} \tag{24}$$

where dT is the temperature increment at the current time step.

(ii) Taking into account the dependence of moisture diffusivity on temperature, water saturation degree, equivalent hydration period and decay of concrete structures, as described in Eq. (3), coupled thermal-hygro-mechanical analysis is performed using the transient thermal-stress analysis in ABAQUS (2004). In the thermal-hygro-mechanical analysis, the shrinkage strain at the $(n+1)$-th time step can be expressed as:

$$\boldsymbol{\varepsilon}_{\text{sh}}^{n+1} = \boldsymbol{\varepsilon}_{\text{sh}}^{n} + \Delta\boldsymbol{\varepsilon}_{\text{sh}} = \boldsymbol{\varepsilon}_{\text{sh}}^{n} + \beta_{\text{sh}}sd\theta\mathbf{I} \tag{25}$$

where $sd\theta$ is the moisture content increment at current time step. The equivalent thermal strain $\boldsymbol{\varepsilon}_{\text{th}}^{\text{eq}(n+1)} = \boldsymbol{\varepsilon}_{\text{th}}^{\text{eq}(n)} + \alpha_T dT\mathbf{I} + \beta_{\text{sh}}sd\theta\mathbf{I}$ can be implemented in the coupled thermal-stress procedure of ABAQUS by using ABAQUS user subroutine to define incremental thermal strains (UEXPAN). In the thermal-hygro-mechanical analysis, the evolutions of the plastic and damage internal state variables are expressed as follows:

$$\boldsymbol{\varepsilon}_{\text{me}}^{n+1} = (\boldsymbol{\varepsilon}_{\text{tot}}^{n} - \boldsymbol{\varepsilon}_{\text{th}}^{n} - \boldsymbol{\varepsilon}_{\text{sh}}^{n}) + (\Delta\boldsymbol{\varepsilon}_{\text{tot}} - \Delta\boldsymbol{\varepsilon}_{\text{th}} - \Delta\boldsymbol{\varepsilon}_{\text{sh}})$$

$$\boldsymbol{\varepsilon}_{\text{pl}}^{n+1} = \boldsymbol{\varepsilon}_{\text{pl}}^{n} + \Delta\boldsymbol{\varepsilon}_{\text{pl}} = \boldsymbol{\varepsilon}_{\text{pl}}^{n} + \Delta\lambda^{n+1}\frac{\partial F^p\left(\bar{\boldsymbol{\sigma}}^{n+1}, \tilde{\boldsymbol{\varepsilon}}_{\text{pl}}^{n+1}\right)}{\partial\bar{\boldsymbol{\sigma}}}$$

$$\tilde{\boldsymbol{\varepsilon}}_{\text{pl}}^{n+1} = \tilde{\boldsymbol{\varepsilon}}_{\text{pl}}^{n} + \mathbf{h}\left(\hat{\bar{\boldsymbol{\sigma}}}, \tilde{\boldsymbol{\varepsilon}}_{\text{pl}}\right) \cdot \Delta\hat{\varepsilon}_{\text{pl}} \tag{26}$$

$$\bar{\boldsymbol{\sigma}}^{n+1} = \mathbf{D}_0^{\text{el}} : \left(\boldsymbol{\varepsilon}_{\text{me}}^{n+1} - \boldsymbol{\varepsilon}_{\text{pl}}^{n+1}\right)$$

$$F^{n+1} = F\left(\bar{\boldsymbol{\sigma}}^{n+1}, \tilde{\boldsymbol{\varepsilon}}_{\text{pl}}^{n+1}\right) = 0$$

The plastic strain $\boldsymbol{\varepsilon}_{\text{pl}}^{n+1}$, the Lagrangian plasticity multiplier $\Delta\lambda^{n+1}$ and the effective stress $\bar{\boldsymbol{\sigma}}^{n+1}$ at the end of the $(n+1)$-th time step can be determined by using the return mapping algorithm [Simo and Hughes (1998); Majorana and Salomoni (2008); Long, Liu and Li (2008)]. Meanwhile, d_t and d_c at the end of the $(n+1)$-th time step can be updated according to Eq. (21). Considering that the evolutions of the uniaxial damage variables d_t and d_c are irreversible processes, d_t and d_c at the $(n+1)$-th time step can be expressed as follows:

$$d_t^{n+1} = \max\left(d_t^{n+1}, d_t^{n}\right)$$
$$d_c^{n+1} = \max\left(d_c^{n+1}, d_c^{n}\right) \tag{27}$$

and the damage variable at the end of the $(n+1)$-th time step can be updated according to Eq. (20). The equivalent hydration period t_e at the end of the $(n+1)$-th time step can be updated as:

$$t_e^{n+1} = t_e^n + \beta_T \beta_h \Delta t \tag{28}$$

where β_T and β_h are the hydration model parameters, Δt represents the length of the current time step.

(iii) Chloride penetration into nonsaturated concrete under combined diffusion and convection mechanisms is performed, considering the dependence of chloride diffusivity on water saturation degree, temperature, time of exposure and the decay of concrete structures, as described in Eq. (9). An iteration algorithm and a successive under-relaxation method are employed to solve the diffusion-convection problem. When the iteration is convergent at the end of chloride penetration analysis, temperature, water saturation degree, damage index and chloride's concentration of each node in the finite element model are updated accordingly, which are applied as input variables for the next time step analysis as illustrated in Fig. 1. Chloride penetration into partially saturated concrete under combined diffusion and convection manners can be implemented by using ABAQUS user subroutine to define an element (UEL).
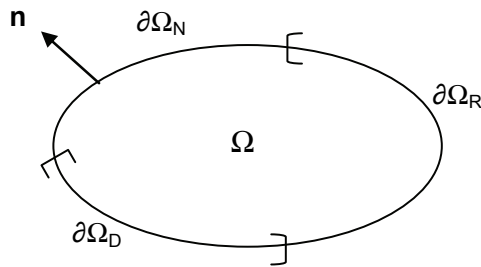
Figure 2: Solution domain and its boundary conditions

4.2 Formulation of the UEL

We consider the following chloride penetration process into nonsaturated concrete on the domain Ω bounded by $\partial \Omega$, as shown in Fig. 2. The governing equation can be expressed as:

$$\frac{\partial C_{tc}}{\partial C_{fc}} \frac{\partial C_{fc}}{\partial t} = \underbrace{\text{div}\left[s D_c \text{grad}\left(C_{fc}\right)\right]}_{\text{diffusion}} + \underbrace{\text{div}\left(s C_{fc} D_\theta \text{grad}\left(\theta\right)\right)}_{\text{convection}} \tag{29}$$

The boundary $\partial\Omega$ is decomposed into a region of Dirichlet boundary conditions $\partial\Omega_D$, Neumann boundary conditions $\partial\Omega_N$ and Robin boundary conditions $\partial\Omega_R$:

$$C_{\text{fc}} = C_{\text{en}} \text{ on } \partial\Omega_D$$
$$J_c^s = sD_c\text{grad}\,(C_{\text{fc}})\cdot\mathbf{n} = q \text{ on } \partial\Omega_N \tag{30}$$
$$J_c^s = sD_c\text{grad}\,(C_{\text{fc}})\cdot\mathbf{n} = sB_c\,(C_{\text{en}} - C_{\text{fc}}) + sC_{\text{en}}B_\theta\,(\theta_{\text{en}} - \theta) \text{ on } \partial\Omega_R$$

where B_c and B_θ are respectively surface chloride and moisture transfer coefficients, C_{en} denotes the chloride concentration of environment, q is the chloride flux through the concrete surface, θ_{en} is the water saturation degree on the boundary and $\mathbf{n}$ denotes the normal direction to the boundary.

Employing the Galerkin weighted residual method on the governing partial differential equation given by Eq. (29) and the boundary conditions given by Eq. (30) yields:

$$\int_\Omega \delta C_{\text{fc}} \left\{ \frac{\partial C_{\text{tc}}}{\partial C_{\text{fc}}}\frac{\partial C_{\text{fc}}}{\partial t} - \underbrace{\text{div}\,[sD_c\text{grad}\,(C_{\text{fc}})]}_{\text{diffusion}} - \underbrace{\text{div}\,[sC_{\text{fc}}D_\theta\text{grad}\,(\theta)]}_{\text{convection}} \right\} d\Omega$$
$$+ \int_{\partial\Omega_N} \delta C_{\text{fc}}\,(J_c^s - q)d\Gamma + \int_{\partial\Omega_R} \delta C_{\text{fc}}\,[J_c^s - sB_c\,(C_{\text{en}} - C_{\text{fc}}) - sC_{\text{en}}D_\theta\,(\theta_{\text{en}} - \theta)]d\Gamma = 0 \tag{31}$$

where δC_{fc} is the weighting function. Using Green's theorem, Eq. (31) can be rewritten as:

$$\int_\Omega \delta C_{\text{fc}} \left\{ \frac{\partial C_{\text{tc}}}{\partial C_{\text{fc}}}\frac{\partial C_{\text{fc}}}{\partial t} + sD_c\text{grad}(\delta C_{\text{fc}})\cdot\text{grad}(C_{\text{fc}}) - sD_\theta\text{grad}(C_{\text{fc}})\cdot\text{grad}(\theta) \right.$$
$$\left. - sC_{\text{fc}}\frac{\partial\theta}{\partial t} \right\} d\Omega \tag{32}$$
$$- \int_{\partial\Omega_N} \delta C_{\text{fc}}q d\Gamma - \int_{\partial\Omega_R} \delta C_{\text{fc}}\,[sB_c\,(C_{\text{en}} - C_{\text{fc}}) + sC_{\text{en}}B_\theta\,(\theta_{\text{en}} - \theta)]d\Gamma = 0$$

Using the finite element method, Eq. (32) can be solved by dividing the domain Ω into elements, in which the field variable is expressed as£°

$$C_{\text{fc}} = N_j C_{\text{fc},j}$$
$$\frac{\partial C_{\text{fc}}}{\partial t} = N_j \dot{C}_{\text{fc},j} \tag{33}$$

where the summation on the repeated index j is implied (here $j = 1, 2, \cdots n_e$), and n_e is the total number of nodes in each element. This convention is referred to as the summation convention of indicial notation (or the Einstein convention). By substituting Eq. (33) into the weak form of Eq. (32), and using the same finite element approximation for θ and $\frac{\partial \theta}{\partial t}$, Eq. (32) can be represented in the matrix form:

$$C_{ij} \dot{C}_{\text{fc},\,j} + K_{ij} C_{\text{fc},\,j} - F_i = 0 \tag{34}$$

where C_{ij}, K_{ij} and F_i are respectively the components of capacitance matrix, property matrix and load vector, and can be expressed as follows:

$$C_{ij} = \sum_e C_{ij}^e \tag{35a}$$

$$K_{ij} = \sum_e K_{ij}^e \tag{35b}$$

$$F_i = \sum_e F_i^e \tag{35c}$$

The components of element capacitance matrix C_{ij}^e, element property matrix K_{ij}^e and element load vector F_i^e can be expressed as:

$$C_{ij}^e = \int_{\Omega^e} \frac{\partial C_{\text{tc}}}{\partial C_{\text{fc}}} N_i N_j d\Omega \tag{36a}$$

$$K_{ij}^e = \int_{\Omega^e} s D_c N_{i,k} N_{j,k} d\Omega - \int_{\Omega^e} s D_\theta N_i \left(N_{l,k} \theta_l \right) N_{j,k} d\Omega - \int_{\Omega^e} s N_i \left(N_l \dot{\theta}_l \right) N_j d\Omega$$
$$+ \int_{\partial \Omega_R^e} s B_c N_i N_j d\Gamma \tag{36b}$$

$$F_i^e = \int_{\partial \Omega_N^e} N_i q d\Gamma + \int_{\partial \Omega_R^e} N_i s \left(B_c C_{\text{en}} + C_{\text{en}} B_\theta \left(\theta_{\text{en}} - \theta \right) \right) d\Gamma \tag{36c}$$

In Eq. (36b), k is a dummy index ($k = 1, 2$ for two dimensions, while $k = 1, 2, 3$ for three dimensions).

Eq. (34) describes a system of first-order differential equations in the time domain. The temporal discretisation is achieved by replacing the time derivative with a finite difference approximation:

$$(\mathbf{C}/\Delta t + \theta \mathbf{K}) \mathbf{C}_{\text{fc}}^{n+1} = (\mathbf{C}/\Delta t - (1 - \theta) \mathbf{K}) \mathbf{C}_{\text{fc}}^n + (1 - \theta) \mathbf{F}^n + \theta \mathbf{F}^{n+1} \tag{37}$$

where θ is a parameter ranging from 0 to 1 and Δt denotes a time increment. Solutions of Eq. (37) obtained for $\theta \geq 0.5$ are known to be unconditionally stable

for a constant time step Δt. The Crank-Nicolson in which $\theta = 0.5$ is usually preferred in numerical implementations since its asymptotic rate of convergence is Δt^2. However, its implementations in chloride transport equation are frequently characterized by oscillations around the correct solutions. In fact, it is observed that large oscillations occur when sudden changes take place in the imposed boundary conditions. The application of the chloride concentration of environment is assuming a step function, wherein chloride ions are applied to the bottom surface of the specimen only during the wetting period, and during the drying period, the chloride flux crossing the concrete surface is set to zero. These oscillations can be reduced to by increasing θ to 1(the backward Euler method). In the present paper, here time integration in transient problem utilizes the backward Euler method. The algorithm is iterative due to the nonlinear nature of the kinetic and diffusivity. A converged solution is deemed to have achieved when:

$$\left| \frac{C_{\text{fc}, l+1}^{n+1} - C_{\text{fc}, l}^{n+1}}{C_{\text{fc}, l}^{n+1}} \right| < \delta \tag{38}$$

at all nodes where δ is a prescribed tolerance and subscript $(l+1)$ is the current iteration number. To stabilize and increase the convergence rate of the iterative procedure in a given time step, a successive under-relaxation method is employed:

$$C_{\text{fc}, l+1}^{n+1} = \omega C_{\text{fc}, l}^{n+1} + (1 - \omega) C_{\text{fc}, l-1}^{n+1} \tag{39}$$

where ω is a constant known as the relaxation factor in the range $0 < \omega < 1$.

5   Computational results and discussions

5.1   Comparisons with analytical results

In order to assess the validity and accuracy of the present computational framework, we consider a steady diffusion-convection problem as illustrated in Fig .3. The governing equation of this problem is given as:

$$\nabla^2 \varphi(\mathbf{x}) - \mathbf{v}(x) \cdot \nabla \varphi(\mathbf{x}) - k\varphi(\mathbf{x}) = 0 \tag{40}$$

The boundary conditions of this problem are those of null flow on the horizontal sides, $q = 0$ at $y = 0$ and $y = 1$, and φ is constant on the vertical sides, $\varphi_a = 300$ at $x = 0$ and $\varphi_b = 10$ at $x = 1$. They are shown graphically in Fig. 3 and can be summarized as follows:

$$\varphi_a = 300 \text{ at } x = 0$$
$$\varphi_b = 10 \text{ at } x = 1$$
$$\frac{\partial \varphi}{\partial \mathbf{n}} = 0 \text{ at } y = 0, y = 1 \tag{41}$$
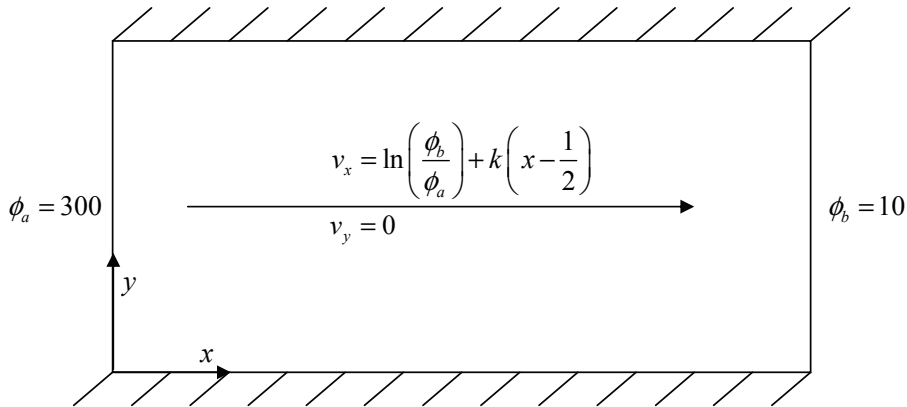
Figure 3: Geometry and boundary conditions for a steady diffusion-convection problem, (Note: ϕ should be φ)

The analytical solution of the problem is given by:

$$\varphi = \varphi_a \exp\left[\frac{kx^2}{2} + \left(\ln\left(\frac{\varphi_b}{\varphi_a}\right) - \frac{k}{2}\right)x\right] \tag{42}$$

The problem is numerically solved here for different values of the constant k. Fig. 4 shows the comparisons between the numerical solutions and the analytical solutions for different values of k, which reveal that the present numerical solutions exactly match the analytical results.

A transient diffusion-convection problem is also chosen here to check the validity and accuracy of the present computational framework. The transient diffusion-convection problem is given as:

$$\frac{\partial C}{\partial t} = u\frac{\partial^2 C}{\partial x^2} - v\frac{\partial C}{\partial x} \tag{43}$$

It is a one dimension problem, and the boundary and initial conditions are graphically shown in Fig. 5 and can be summarized as follows:

$$
\begin{aligned}
C(x,0) &= 0, \quad x > 0 \\
C(0,t) &= C_0, \quad t > 0 \\
C(\infty,t) &= 0, \quad t > 0
\end{aligned}
\tag{44}
$$

The analytical solution for the transient diffusion-convection problem is given as:

$$C(x,t) = \frac{C_0}{2}\left[\exp\left(\frac{v}{u}x\right)\mathrm{erfc}\left(\frac{x}{2\sqrt{ut}} + \frac{v\sqrt{ut}}{2u}\right) + \mathrm{erfc}\left(\frac{x}{2\sqrt{ut}} - \frac{v\sqrt{ut}}{2u}\right)\right] \tag{45}$$
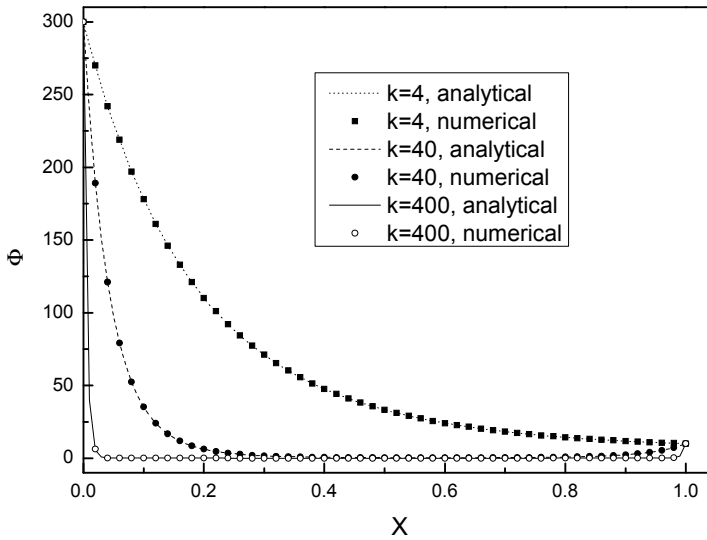
Figure 4: Comparisons of analytical results and numerical solutions for different values of *k*
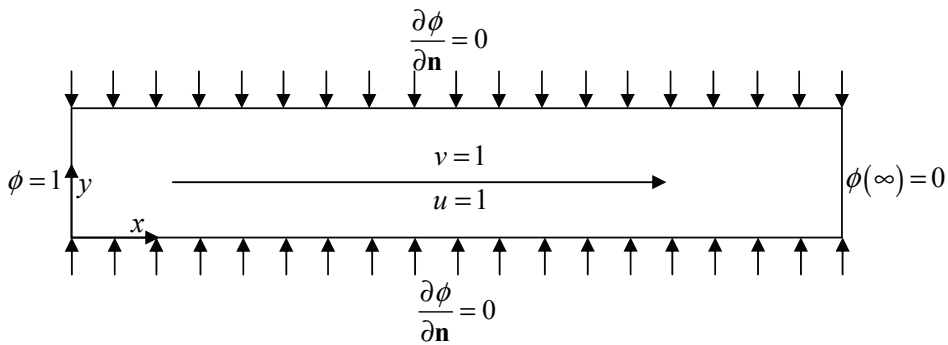
Figure 5: Geometrical configuration and boundary conditions for a transient diffusion-convection problem

The comparisons between analytical solutions and numerical solutions at different time points are illustrated in Fig. 6, which show the validity and accuracy of the present computational framework. It can be derived that the computational framework can be extended to more complex situations for modeling chloride penetration into nonsaturated RC structures under combined diffusion and convection mecha-
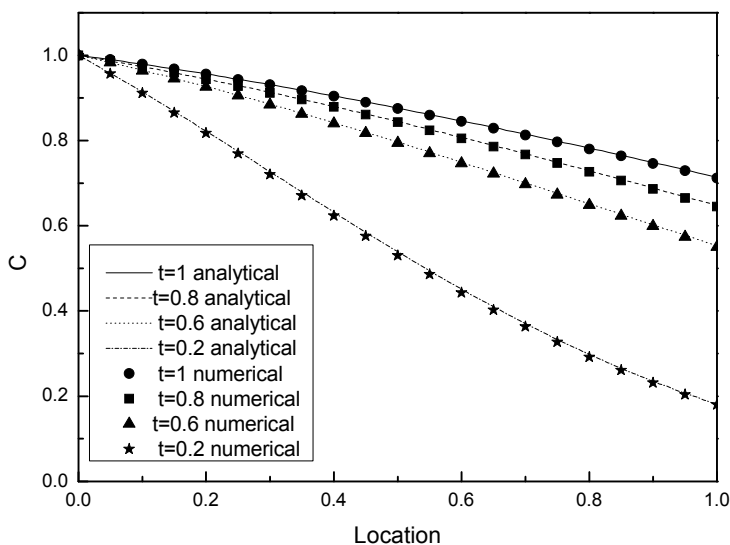
Figure 6: Comparisons of analytical results and numerical solutions at various time points

nisms.

5.2 *Comparisons with experimental data*

To view the ability of the proposed computational framework to predict real chloride penetration data, comparisons of computational results and experimental observations are conducted. The experimental results were obtained from 126 days chloride penetration into concrete under different drying and wetting cycles [Li (2009)]. In the experimental test, four groups of specimens (100mm × 100mm × 100mm cubes) were used to observe chloride penetration into concrete specimens under different drying and wetting cycles. All faces of these specimens, except one, were protected with epoxy paint so that chloride penetration into concrete could take place through one face only. The first group was exposed to 1 mol/L NaCL solution for 126 days, while the other three groups were exposed to a series of different drying-wetting cycles, as illustrated in Fig. 7. The material properties of concrete in the experimental test are given as follows: the porosity of concrete $s = 0.161$, the chloride diffusivity $D_c = 7.92 \times 10^{-12} \mathrm{m^2/s}$, the moisture diffusivity during drying period $D_d^s = 1.31 \times 10^{-10} \mathrm{m^2/s}$, and the moisture diffusivity during wetting period $D_w^0 = 4.05 \times 10^{-11} \mathrm{m^2/s}$. Fig. 8 shows the comparisons of

the total chloride concentration predicted by the present computational framework and those observed by experiment. It can be seen that the results predicted by the present computational framework agree well with the test data for chloride penetration into partially saturated concrete structures under different drying and wetting cycles. The validity of the proposed implementation to model chloride ingress into partially saturated concrete is confirmed.
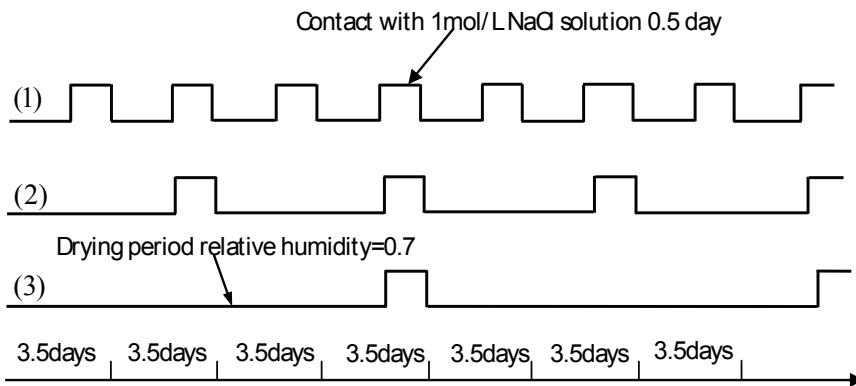
Figure 7: Different drying-wetting cyclic periods

5.3 *Applications of the proposed computational framework*

Traditional models for predicting service life of RC structures exposed to chloride environment are focused on chloride penetration without considering the coupling between mass transport and multiple deterioration processes and the difference of moisture transport during drying-wetting cycles, which frequently occur in field applications. In the present paper, an initially chloride-free and simply supported RC specimen under service loadings illustrated in Fig. 9 is chosen to implement the proposed computational framework which takes environment temperature and humidity fluctuations, diffusion and convection, chloride binding, as well as the decay of durability of structures caused by coupled deterioration processes into account. Only the bottom surface of the specimen is exposed to chloride during the wetting period, as illustrated in Fig. 9. The value of parameter C_{en}, i.e., the amount of applied chloride coming from sea water, is evaluated in the present computational framework by assuming a step function, wherein chloride ions are applied to the bottom surface of the specimen only during the wetting period, as illustrated in Fig. 10. During the drying period, the chloride flux crossing the concrete surface is set to zero since chloride ions will remain in the concrete unless washing-away effects
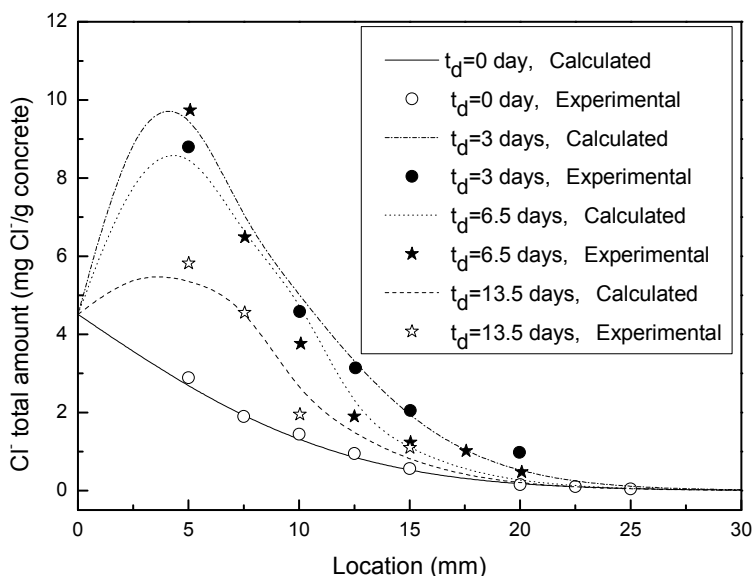
Figure 8: Comparisons of chloride profiles predicted by the present framework and those tested by experiment

are taken into account. To consider the seasonal variation of ambient temperature, the annual variation of ambient temperature can be assumed as a sinusoidal function [Saetta, Scotta and Vitaliani (1993)]:

$$T_{en} = 15 + 15\sin(2\pi t) \tag{46}$$

where T_{en} is the ambient temperature (°), t is the time of exposure (years). The material properties of the concrete specimen are described in detail in Table 2.

X-symmetry conditions allow us to model half of the concrete specimen and the mesh of the specimen is illustrated in Fig. 11. The free chloride profiles after an exposure of 50 years predicted by the present computational framework are shown in Fig. 12, where the depth of penetration is measured from the exposed surface of the concrete specimen, and the length is measured from the supported position of the specimen illustrated in Fig. 9. From Fig. 12, it can be seen that the free chloride concentration reaches a maximum value about 10∼15 mm inside the concrete, which correspond with field observations [Andrade and Alonso (1996)] and beyond this depth the free chloride concentration decreases with increase in the depth from the exposed surface. It also shows that at the same depth, the free chloride concentration increases with increase in the length, which is confirmed by
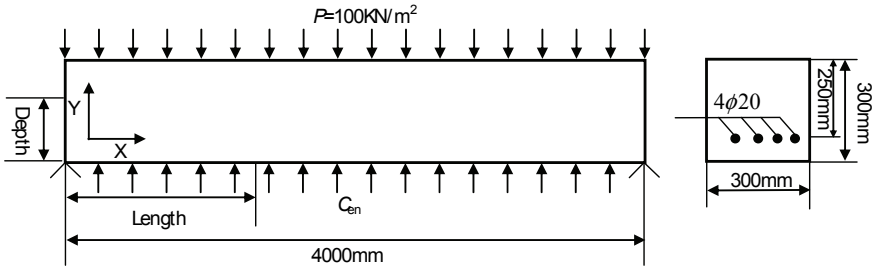
Figure 9: Geometry and boundary conditions of the concrete specimen
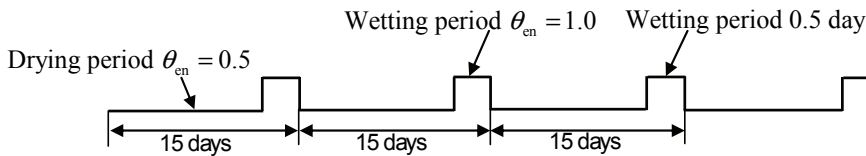
Figure 10: Drying-wetting cycles

Table 2: Values of material properties of concrete used for the numerical analysis

Properties	Value
Porosity s	0.10
Reference chloride diffusivity (m²/s) $D_{c, ref}$	2.0×10^{-12}
Moisture diffusivity during drying period(m²/s) D_d^s	2.0×10^{-10}
Moisture diffusivity during wetting period(m²/s) D_w^0	3.22×10^{-10}
Density of concrete ρ(kg/m³)	2400
Special heat capacity(W/m.K) c	1000
Thermal expansion coefficient(1/K) α_T	1.0×10^{-5}
Shrinkage coefficient β_{sh}	9.96×10^{-3}
Environment chloride concentration (mol/l) C_{en}	0.5
Initial Elastic Modulus (GPa) E	27
Compression strength (MPa) f_{c0}	30
Tensile strength (MPa) f_{t0}	3.3
Dilation constant γ_p	0.7813
Material parameters κ_t	1.5×10^3
Material parameters κ_c	0.5×10^3
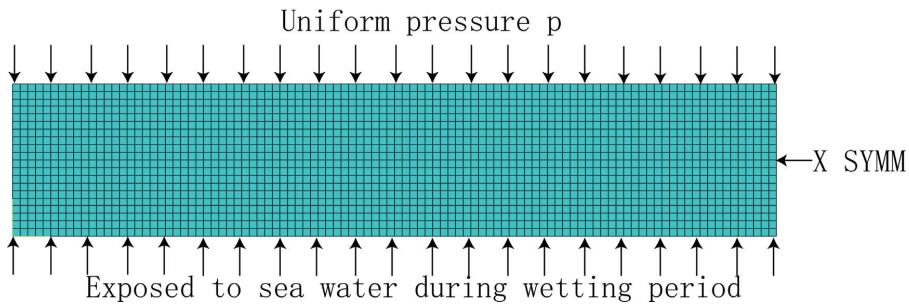
Figure 11: Finite element model of the concrete specimen
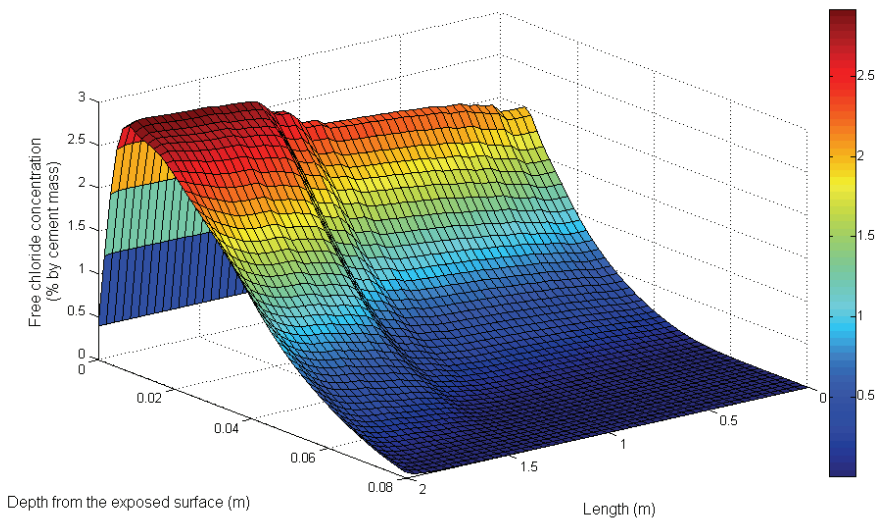
Figure 12: Chloride profiles after 50 years of exposure

experimental observations [Yoon Wang, Weiss and Shah (2000)]. This is because the damage variable increases with increase in the length as illustrated in Fig. 17 and results in an increase of chloride diffusivity. Service life predictions can be obtained by assuming that the service life of a RC structure exposed to chloride environment corresponds to the period until reinforcement depassivation. The free chloride threshold concentration used is 0.2% by mass of cemetiotious material (ACI, 2002). It can be seen from Fig. 13 that, in order to assure the initiation time of reinforcement corrosion beyond 50 years under multi-deterioration processes,
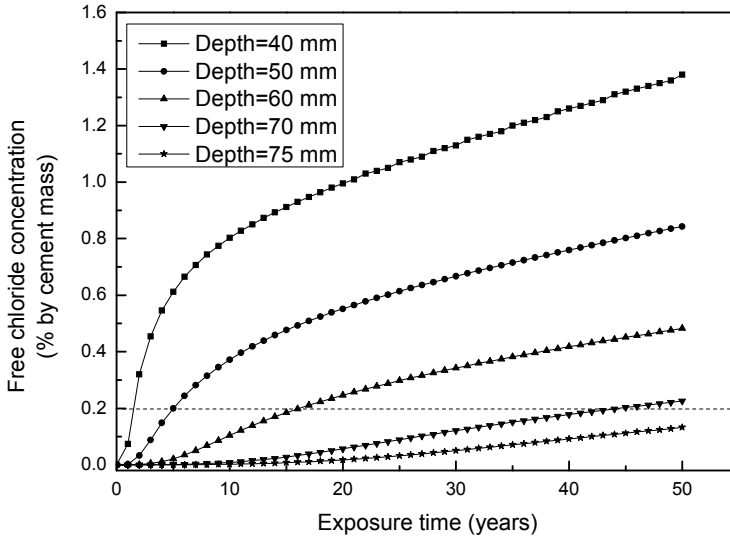
Figure 13: Time profile of free chloride concentration
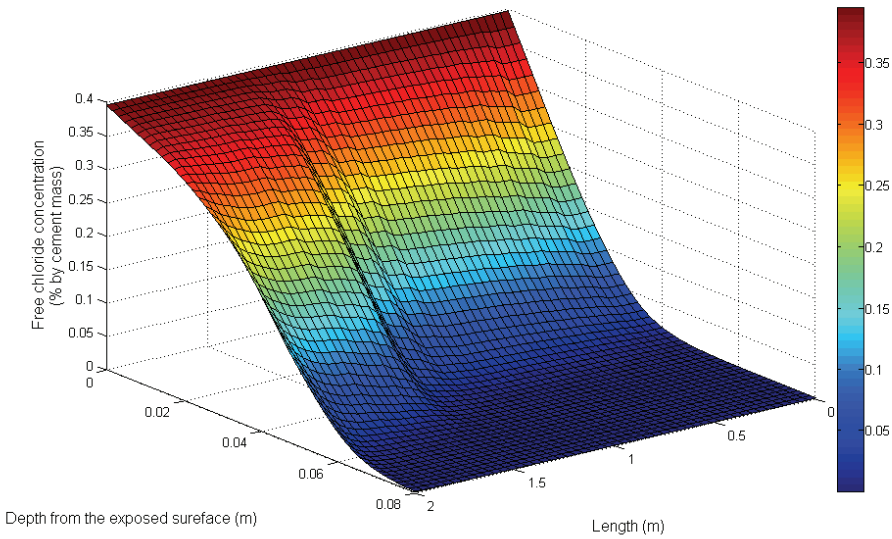
Figure 14: Chloride profiles after 50 years of exposure in the situation of neglecting convection
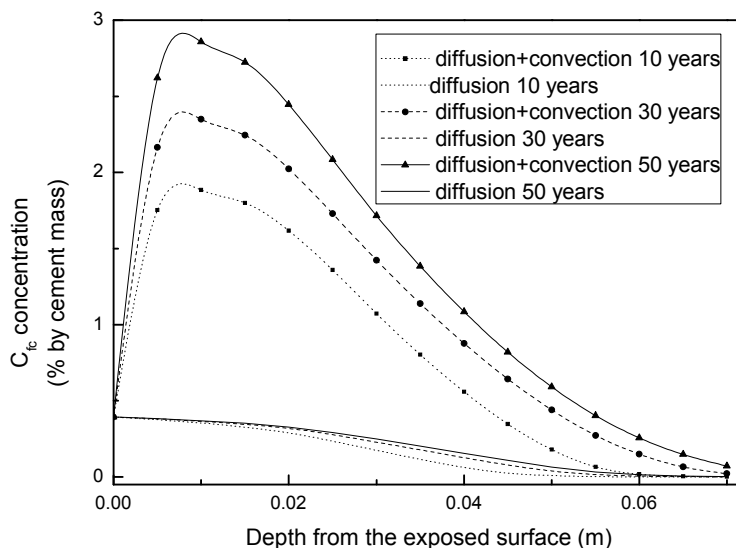
Figure 15: Effect of convection on free chloride profiles

the thickness of concrete cover should not be less than 75 mm.

In order to study the effects of convection, decay of structures and the chloride binding capacity on service life of RC structures exposed to chloride environment, comparisons of the chloride profiles predicted by the present computational framework and those predicted by these models which neglect some factor are conducted in the following.

5.3.1 *Influence of convection on chloride profiles*

Chloride transport into partially saturated concrete structures is a complex phenomenon, driven by non-uniform distribution of chloride ions (i.e., diffusion) and moisture transport (i.e., convection). The latter process conveys a greater quantity of chloride ions than the pure diffusion process, and therefore can't be ignored. The effect of convection on chloride profiles is researched by analyzing two different cases: the one in which chloride penetration into concrete is driven by diffusion only, while the second one in which chloride penetration into concrete is driven by combined diffusion and convection. The free chloride profiles after an exposure of 50 years under diffusion only are shown in Fig. 14. It can be seen that the free chloride concentration decreases with increase in the depth from the exposed surface. The plots of free chloride concentration versus depth in the middle span of the specimen after 10 years, 30 years and 50 years of exposure for the two cases

are shown in Fig. 15. It can be observed that, at any fixed depth, the free chloride concentration for the second case is much greater than that for the first case. This is due to the coupled moisture diffusion and chloride penetration, which is shown in Eq. (29). The coupling effect contributes significantly to chloride penetration into partially saturated concrete. In order to assure the initiation time of reinforcement corrosion beyond 50 years under diffusion only, the thickness of concrete cover should not be less than 45 mm, as illustrated in Fig. 16, while that should not be less than 75 mm under combined diffusion and convection. It can be concluded that neglecting the effect of convection on chloride ingress into non-saturated concrete overestimates service life of RC structures, and this point may be essential for durability design and assessment of RC structures in the splash and tidal zones or of highway concrete structures exposed to de-icing salts.
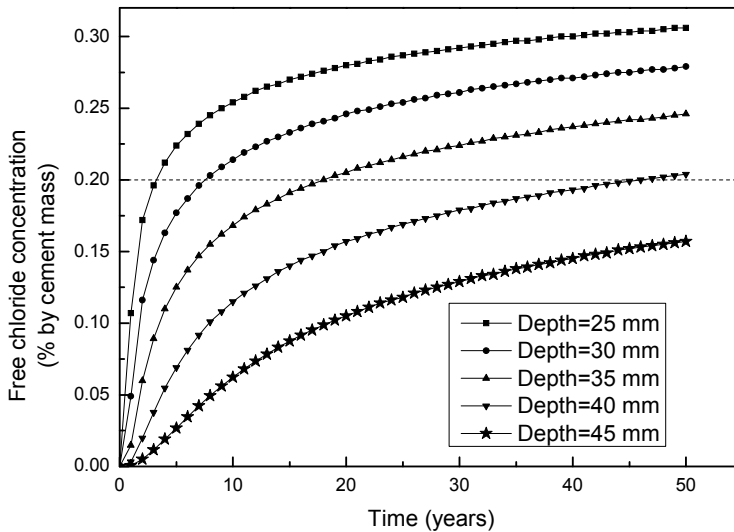
Figure 16: Time profile of free chloride concentration in the situation of neglecting convection

5.3.2 *Influence of decay on chloride profiles*

Most deterioration processes alter the porosity and permeability of concrete, trigger the initiation and evolution of damage, impair the durability of RC structures and thus result in accelerating aggressive agents' penetration into RC structures. In turn, the durability of RC structures decays further due to the accelerating deterioration processes. The coupling between mass transport and multi-deterioration

damage variable

+5.844e−01
+5.357e−01
+4.870e−01
+4.383e−01
+3.896e−01
+3.409e−01
+2.922e−01
+2.435e−01
+1.948e−01
+1.461e−01
+9.740e−02
+4.870e−02
+0.000e+00

Figure 17: Damage distribution after 50 years of exposure
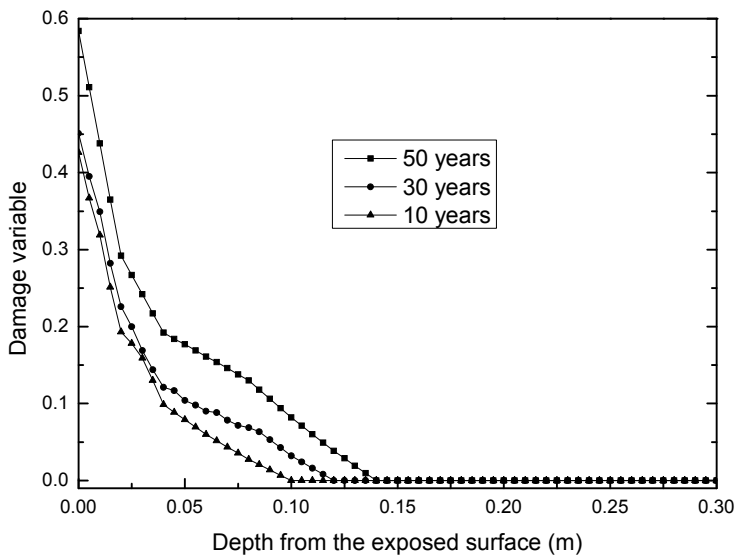
Figure 18: Damage variable versus depth at different time points

processes is becoming increasingly necessary to be considered in durability design and assessment of RC structures.

The alteration of the porosity and permeability of concrete can be taken into account by introducing a scalar damage variable into the present computational framework. The influence of the decay of RC structures on mass transport is considered
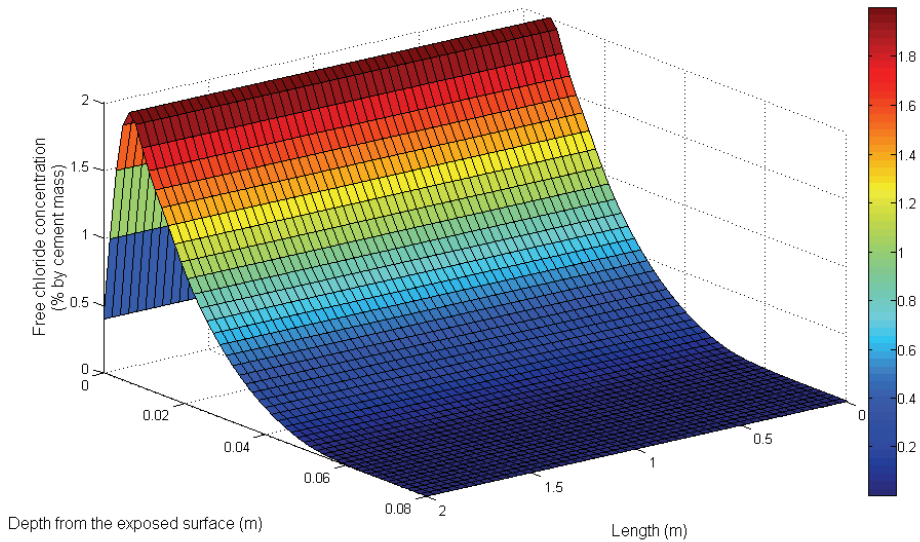
Figure 19: Free chloride profiles after 50 years of exposure in the situation of neglecting decay

by modifying respectively mass diffusion coefficients, as shown in Eq. (3) and Eq. (9). The effect of the decay of concrete structures on chloride profiles is studied by analyzing two different cases: the first one in which the decay of concrete structures is neglected, while the second one in which the decay of concrete structures is taken into account by introducing a scalar damage index. The damage variable distribution after 50 years of exposure is illustrated in Fig. 17. As expected, the damage variable reaches a maximum value at the bottom surface of the middle span of the specimen, where there is the largest tension strain. The damage variable in the middle span of the specimen versus time is illustrated in Fig. 18. It can be observed that the decay of the specimen is increasing due to the coupling between mass transport and various deterioration processes. The free chloride profiles after an exposure period of 50 years in the situation of neglecting decay are shown in Fig. 19. It can be seen that the free chloride concentration in this situation isn't relevant to the stress state of the specimen. The plots of free chloride concentration versus depth in the middle span of the specimen after 10 years, 30 years and 50 years of exposure for the two cases are shown in Fig. 20. As expected, the free chloride concentration for the second case is higher than that for the first case. It can be observed from Fig. 21 that, in order to assure the initiation time of rein-
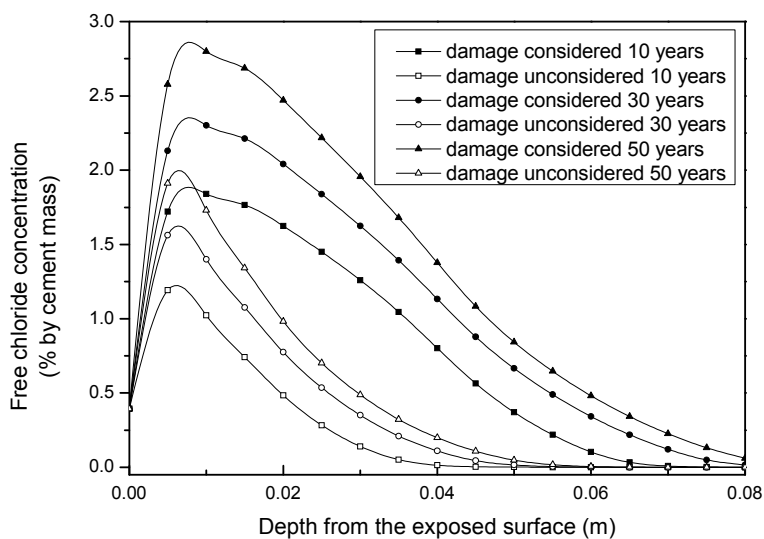
Figure 20: Influence of the decay of concrete structures on free chloride profiles

forced steel corrosion beyond 50 years, the thickness of concrete cover should not be less than 45 mm in the situation of neglecting the decay of concrete structures, while that should not be less than 75 mm when the decay of concrete structures is taken into account.

5.3.3 *Influence of chloride binding capacity on chloride profiles*

Chloride ions in concrete structures can be either dissolved in the pore solution (free chloride ions), or chemically and physically bound to the cement hydrates and their surfaces (bound chloride ions). Chloride-induced corrosion is related only to the free chloride, since the bound chloride ions are immovable and don't initiate reinforcement corrosion. However, the bound chloride ions exert a tremendous effect on the free chloride penetration into concrete. The effect of binding isotherm nature on the free chloride profiles is studied by analyzing two different cases: the first one in which binding is neglected, and the second one in which a nonlinear Freundlich binding isotherm is adopted (α=1.037, β=0.36). The free chloride profiles in the situation of neglecting binding effect are shown in Fig. 22 which is similar to Fig. 12. The plots of free chloride concentration versus depth at the middle span of the specimen after 10, 30 and 50 years of exposure for the two cases are illustrated in Fig. 23. As expected, the free chloride concentration for the second case is lower than that for the first case. From Fig. 24, In order to assure the initiation time of re-
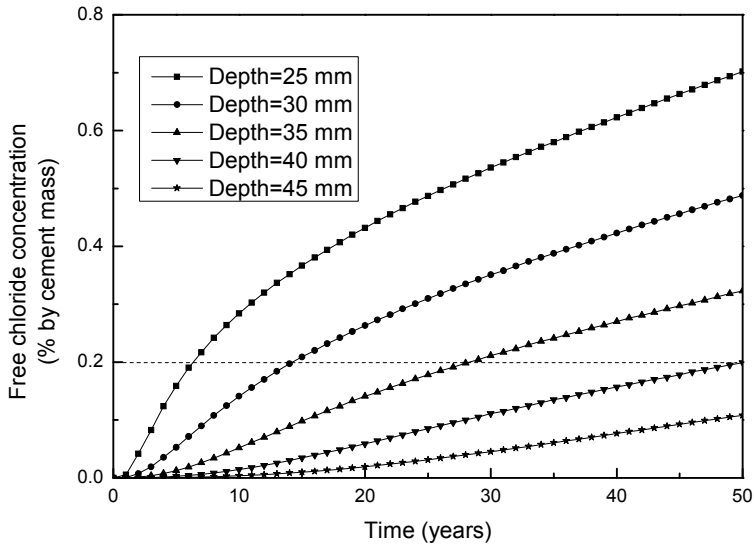
Figure 21: Time profile of free chloride concentration in the situation of neglecting decay
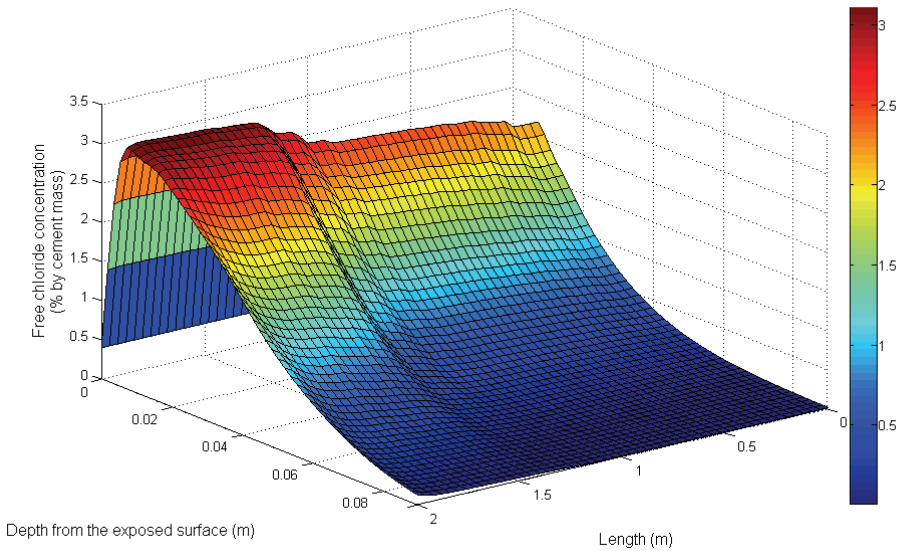
Figure 22: Chloride profiles after 50 years of exposure in the situation of neglecting binding effect
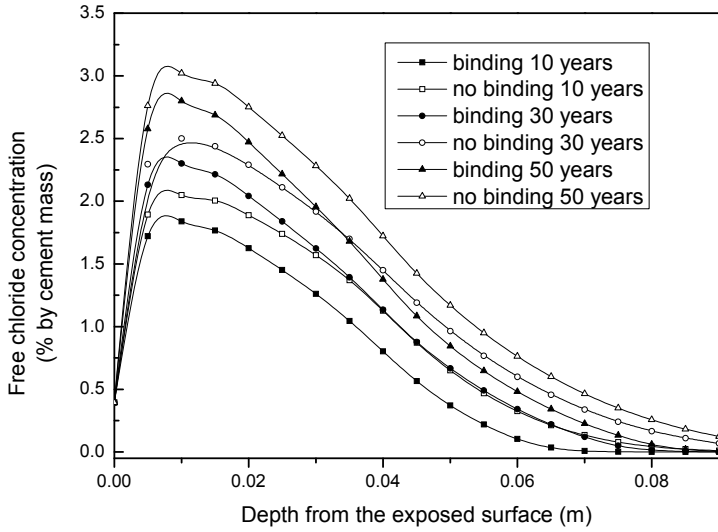
Figure 23: Influence of binding effect on free chloride profiles
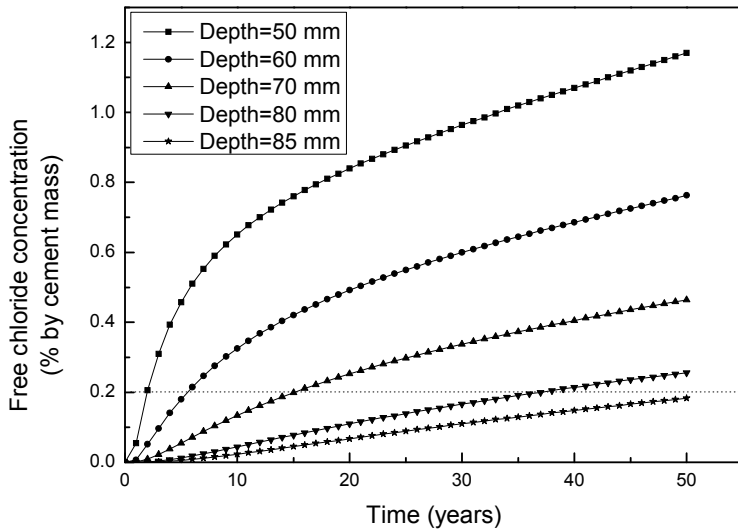
Figure 24: Time profile of free chloride concentration in the situation of neglecting binding effect

inforcement corrosion beyond 50 years, the thickness of concrete cover should not be less than 85 mm in the situation of neglecting binding effect, while that should not be less than 75 mm in the situation of taking binding effect into account. It can be concluded from the above analyses that improving the binding chloride capacity of concrete can extend significantly service life of concrete structures.

6 Conclusions

An integrated finite element-based computational framework is developed in this paper for predicting service life of RC structures exposed to chloride environment, which takes environment temperature and humidity fluctuations, diffusion and convection, chloride binding, as well as the decay of structures caused by coupled deterioration processes into account. The resulting system of governing equations, in terms of temperature, water saturation degree and free chloride concentration, are solved numerically by the Galerkin finite element method to describe spatial variations and a finite difference recurrence relationship for the temporal discretization. The validity and accuracy of the present computational framework are confirmed by comparing the computational results with the analytical solutions and experimental observations. The present study and analysis enable the following conclusions to be drawn:

(1) The difference of moisture transport into concrete during drying and wetting periods and the effect of moisture migration on chloride penetration into non-saturated concrete structures have been incorporated in the present computational framework. From a physical point of view, this is in better agreement with reality than the traditional models which only consider pure diffusion. It appears that in case of a drying-wetting exposure, such as in the tidal and splash zones of marine concrete structures and in de-icing salt environments, the chloride profiles predicted by the present computational framework differ substantially from those predicted by the traditional models. The validation of the present computational framework is verified by experimental and filed observations. This shows the need for an evaluation of the service life of RC structures exposed to drying and wetting cycles on the basis of the present computational framework.

(2) Most deterioration processes alter the porosity and permeability of concrete and result in accelerating aggressive agents' penetration into concrete. It seems that, for concrete structures under multi-deterioration processes, the chloride profiles predicted by the present framework are related to the decay of RC structures while those traditional models are unrelated to the decay of RC structures. Experimental and field observations show that service life of RC structures is related to the decay of durability of structures. It shows the need for prediction of service life of RC concrete structures subjected to various deterioration processes on the basis of the

present computational framework.

(3) The bound chloride exerts a tremendous influence on chloride ingress into concrete structures, and this would reduce free chloride concentration near the reinforcement and could extend concrete structures' service life. Consequently improving chloride binding capacity of concrete can prolong service life of concrete structures exposed to chloride environment.

References

Ababneh, A.; Benboudjema, F.; Xi, Y. (2003): Chloride Penetration in Nonsaturated Concrete. *Journal of Materials in Civil Engineering*. Vol.15, pp. 183-191.

ABAQUS Version 6.5. (2004): Hibbitt, Karlsson and Sorensen Inc., Pawtucket.

Aldea, C. M.; Shah, S. P.; Karr, A. (1999): Permeability of cracked concrete. *Materials and Structures* Vol. 32, pp. 370-376.

American Concrete Institute. (2002): Corrosion of Metals in Concrete. ACI manual of concrete practice. ACI Committee 222R-01.

Andrade, C.; Alonso, C. (1996): Progress on design and residual life calculation with regard to rebar corrosion in reinforced concrete. Techniques to assess the corrosion activity of steel reinforced concrete structures, ASTM STP 1276. Philadelphia, PA, USA, 1996.

Bangert, F.; Grasberger, S.; Kuhl, D.; Meschke, G. (2003): Environmentally induced deterioration of concrete: physical motivation and numerical modeling. *Engineering Fracture Mechanics*. Vol. 70, pp. 891-910.

Bazant, Z. P.; Najjar, L. J. (1972): Nonlinear water diffusion in nonsaturated concrete. *Materials and Structures*. Vol. 5, pp. 3-20.

Cerny, R.; Drchalova, J.; Rovnanikova, P. (2001): The effects of thermal load and frost cycles on the water transport in two high-performance concretes. *Cement and Concrete Research*. Vol. 31, pp. 1129-1140.

Chen, D.; Mahadevan, S. (2007): Cracking Analysis of Plain Concrete under Coupled Heat Transfer and Moisture Transport Processes. *Journal of Structural Engineering-ASCE*. Vol. 133, pp. 400-410.

Chen, Z.; Gan, Y.; Chen, J. K. (2008): A coupled thermo-mechanical model for simulating the material failure evolution due to localized heating. *CMES: Computer Modeling in Engineering and Sciences*. Vol. 26, pp. 123-137.

Ciampoli, M. (1999): A probabilistic methodology to assess the reliability of deteriorating structural elements. *Computer Methods in Applied Mechanics and Engineering.* Vol. 168, pp. 207-220.

Cicekli, U.; Voyiadjis, G. Z.; Abu Al-Rub, R. K. (2007): A plasticity and anisotropic damage model for plain concrete. *International Journal of Plasticity.* Vol. 23, pp 1874-1900.

Djerbi, A.; Bonnet, S.; Khelidj, A.; Baroghel-bouny, V. (2008): Influence of traversing crack on chloride diffusion into concrete. *Cement and Concrete Research.* Vol. 38, pp. 877-883.

Ferguson, W. J.; Palananthakumar, B. (2005): A fully coupled finite element model of landfill gas migration in a partially saturated soil. *CMES: Computer Modeling in Engineering and Sciences.* Vol. 8: 201-215.

Francois, R.; Maso, J. C. (1988): Effect of damage in reinforced concrete on carbonation or chloride penetration. *Cement and Concrete Research.* Vol. 18, pp. 961-970.

Gawin, D; Pesavento, F; Schrefler, B. A. (2006a): Hygro-thermo-chemo -mechanical modelling of concrete at early ages and beyond. Part I: Hydration and hygrothermal phenomena. *International Journal for Numerical Methods in Engineering.* Vol. 67, pp. 299-331.

Gawin, D; Pesavento, F; Schrefler, B. A. (2006b): Hygro-thermo-chemo -mechanical modelling of concrete at early ages and beyond. Part II: Shrinkage and creep of concrete. *International Journal for Numerical Methods in Engineering.* Vol. 67, pp. 332-363.

Gerard, B.; Pijaudier-Cabot, G.; Laborderie, C. (1998): Coupled diffusion-damage modelling and the implications on failure due to strain localisation. *International Journal of Solids and Structures.* Vol. 35, pp. 4107-4120.

Gerard, B.; Marchand, J. (2000): Influence of cracking on the diffusion properties of cement-based materials: Part I: Influence of continuous cracks on the steady-state regime. *Cement and Concrete Research.* Vol. 30, pp. 37-43.

Golberg, M. A.; Chen, C. S. (2001): An efficient mesh-free method for nonlinear reaction-diffusion equations. *CMES: Computer Modeling in Engineering and Sciences.* Vol. 2, pp. 87-95.

Gomez, H.; Colominas, I.; Navarrina, F.; Casteleiro, M. (2007): A discontinuous Galerkin method for a hyperbolic model for convection-diffusion problems in CFD. *International Journal for Numerical Methods in Engineering.* Vol. 71, pp. 1342-1364.

Isgor, O. B.; Razaqpur, A. G. (2004): Finite element modeling of coupled heat

transfer, moisture transport and carbonation processes in concrete structures. *Cement and Concrete Composites.* Vol. 26, pp. 57-73.

Janssen, H.; Blocken, B.; Carmeliet, J. (2007): Conservative modelling of the moisture and heat transfer in building components under atmospheric excitation. *International Journal of Heat and Mass Transfer.* Vol. 50, pp. 1128-1140.

Kringos, N.; Scarpas, A.; Selvadurai, A. P. (2008): Simulation of mastic erosion from open-graded asphalt mixes using a Hybrid Lagrangian-Eulerian finite element approach. *CMES: Computer Modeling in Engineering & Sciences*, Vol, 28, no. 3, pp. 147-159.

Lee, J.; Fenves, G. L. (1998): Plastic-damage model for cyclic loading of concrete structures. *Journal of Engineering Mechanics-ASCE.* Vol. 124, pp. 892-900.

Li, C.Q. (2009): Water and ionic transport processes in cover concrete under drying-wetting cycles. PhD thesis. Tsinghua university(China), Beijing.

Lin, H.; Atluri, S. N. (2000): Meshless local Petrov-Galerkin (MLPG) method for convection-diffusion problems. *CMES: Computer Modeling in Engineering and Sciences.* Vol.1, pp. 45-60.

Long, S. Y.; Liu, K. Y.; Li, G. Y. (2008): An analysis for the elasto-plastic fracture problem by the meshless local Petrov-Galerkin method. *CMES: Computer Modeling in Engineering & Sciences*, Vol, 28, no. 3, pp. 203-216.

Mai-Duy, N.; Tran-Cong, T.; Tanner, R. I. (2006): A new high-order time-kernel BIEM for the Burgers equation. *CMES: Computer Modeling in Engineering & Sciences*, Vol, 16, no. 3, pp. 177-186.

Majorana, C. E.; Salomoni, V. A. (2008): Dynamic Nonlinear Material Behaviour of Thin Shells in Finite Displacements and Rotations. *CMES: Computer Modeling in Engineering & Sciences*, Vol, 33, no. 1, pp. 49-84.

Martín-Pérez, B.; Zibara H.; Hooton, R. D.; Thomas, M. D. A. (2000): A study of the effect of chloride binding on service life predictions. *Cement and Concrete Research.* Vol. 30, pp. 1215-1223.

Martín-Pérez, B.; Pantazopoulou, S. J.; Thomas, M. D. A. (2001): Numerical solution of mass transport equations in concrete structures. *Computers & Structures.* Vol. 79, pp. 1251-1264.

Masi, M.; Colella, D.; Radaelli, G.; Bertolini, L. (1997): Simulation of chloride penetration in cement-based materials. *Cement and Concrete Research.* Vol. 27, pp. 1591-1601.

Mohammadi, M. H. (2008): Stabilized Meshless Local Petrov-Galerkin (MLPG) method for incompressible viscous fluid flows. *CMES: Computer Modeling in Engineering & Sciences*, Vol, 29, no. 2, pp. 75-94.

Petryna, Y. S.; Kratzig, W. B. (2005): Computational framework for long-term reliability analysis of RC structures. *Computer Methods in Applied Mechanics and Engineering*. Vol. 194, pp. 1619-1639.

Roels, S.; Moonen, P.; Proft, K. D.; Carmeliet, J. (2006): A coupled discrete-continuum approach to simulate moisture effects on damage processes in porous materials. *Computer Methods in Applied Mechanics and Engineering.* Vol. 195, pp. 7139-7153.

Romero, L. M.; Benitez, F. G. (2008): A boundary element numerical scheme for the two-dimensional convection-diffusion equation. *International Journal for Numerical Methods in Engineering*. Vol. 76, pp. 2063-2090.

Saetta, A. V.; Scotta, R. V.; Vitaliani, R. V. (1993): Analysis of Chloride Diffusion into Partially Saturated Concrete. ACI Materials Journal. Vol. 90, pp. 441-451.

Samaha, H. R.; Hover, K. C. (1992): Influence of microcracking on the mass transport properties of concrete. *ACI Materials Journal.* Vol. 89, pp. 416-424.

Samson, E.; Marchand, J.; Robert, J. L.; Bournazel, J. P. (1999): Modelling ion diffusion mechanisms in porous media. *International Journal for Numerical Methods in Engineering*. Vol. 46, pp. 2043-2060.

Selvadurai, A. P.; Dong, W. J. (2006): Time adaptive scheme for the solution of the advection equation in the presence of a transient flow velocity. *CMES: Computer Modeling in Engineering and Sciences*. Vol. 12, pp. 41-53.

Simo, J. C.; Hughes, T. J. R. (1998): Computational inelasticity. Springer-Verlag, New York.

Simoes, N.; Tadeu, A. (2005): 3D transient heat transfer by conduction and convection across a 2D medium using a boundary element model. *CMES: Computer Modeling in Engineering and Sciences*. Vol. 9, pp. 221-233.

Tabrez, S.; Mitra, M.; Gopalakrishnan, S. (2007): Modeling of degraded composite beam due to moisture absorption for wave based detection. *CMES: Computer Modeling in Engineering and Sciences*. Vol. 22, pp. 77-89.

Tang, L.; Nilsson L. O. (1993): Chloride binding capacity and binding isotherms of OPC pastes and mortars. *Cement and Concrete Research.* Vol. 23, pp. 247-253.

Wong, S. F.; Wee, T. H.; Swaddiwudhipong, S.; Lee, S. L. (2001): Study of water movement in concrete. *Magazine of Concrete Research.* Vol. 53, pp. 205-220.

Yoon, S.; Wang, K.; Weiss, W. J.; Shah, S. P. (2000): Interaction between Loading, Corrosion, and Serviceability of Reinforced Concrete. *ACI Materials Journal.* Vol. 97, pp. 637-644.